A dusty star-forming galaxy at z = 6 revealed by strong gravitational lensing

Zavala, J.A.; Montaña, A.; Hughes, D.H.; Yun, M.S.; Ivison, R.J.; Valiante, E.; ... ; Zeballos, M.

An amplified dusty star-forming galaxy at *z*=6: unveiling an elusive population of galaxies

Jorge A. Zavala[1*], Alfredo Montaña[2], David H. Hughes[1], Min S. Yun[3], R. J. Ivison[4,5], Elisabetta Valiante[6], David Wilner[7], Justin Spilker[8], Itziar Aretxaga[1], Stephen Eales[6], Vladimir Avila-Reese[9], Miguel Chávez[1], Asantha Cooray[10], Helmut Dannerbauer[11,12], James S. Dunlop[5], Loretta Dunne[5,6], Arturo I. Gómez-Ruiz[2], Michał J.Michałowski[13], Gopal Narayanan[3], Hooshang Nayyeri[10], Ivan Oteo[5,4], Daniel Rosa González[1], David Sánchez-Argüelles[1], Stephen Serjeant[14], Matthew W. L. Smith[6], Elena Terlevich[1], Olga Vega[1], Alan Villalba[1], Paul van der Werf[15], Grant W. Wilson[3], Milagros Zeballos[1]

[1]*Instituto Nacional de Astrofísica, Óptica y Electrónica (INAOE), Luis Enrique Erro 1, 72840, Puebla, Mexico*
[2]*CONACYT-Instituto Nacional de Astrofísica, Óptica y Electrónica, Luis Enrique Erro 1, 72840, Puebla, Mexico*
[3]*Department of Astronomy, University of Massachusetts, MA 01003, USA*
[4]*European Southern Observatory, Karl Schwarzschild Strasse 2, Garching, Germany*
[5]*Institute for Astronomy, University of Edinburgh, Royal Observatory, Blackford Hill, Edinburgh EH9 3HJ, UK*
[6]*School of Physics and Astronomy, Cardiff University, The Parade, Cardiff CF24 3AA, UK*
[7]*Harvard-Smithsonian Center for Astrophysics, 60 Garden Street, Cambridge, MA 02138, USA*
[8]*Steward Observatory, University of Arizona, 933 North Cherry Avenue, Tucson, AZ 85721, USA*
[9]*Instituto de Astronomía, Universidad Nacional Autónoma de México, A.P. 70-264, 04510, CDMX, Mexico*
[10]*Dept. of Physics & Astronomy, University of California, Irvine, CA 92697, USA*
[11]*Instituto de Astrofísica de Canarias (IAC), E-38205 La Laguna, Tenerife, Spain*
[12]*Universidad de La Laguna, Dpto. Astrofísica, E-38206 La Laguna, Tenerife, Spain*
[13]*Astronomical Observatory Institute, Faculty of Physics, Adam Mickiewicz University, ul. Słoneczna 36, 60-286 Poznań, Poland*
[14]*Department of Physical Sciences, The Open University, Milton Keynes, MK7 6AA, UK*
[15]*Leiden Observatory, Leiden University, P.O. Box 9513, NL-2300 RA Leiden, The Netherlands*

Since their discovery, submillimeter-selected galaxies[1,2] (SMGs) have revolutionized the field of galaxy formation and evolution. Hundreds of square degrees have been mapped at submillimeter wavelengths[3–5] and notwithstanding the negative K-correction in the submm bands[6], where there is no significant loss of sensitivity to the detection of these sources up to $z \sim 10$, only a handful of sources have been confirmed to lie at $z > 5$ (ref.[7–11]) and only two at $z \geq 6$ (ref.[12,13]). All of these SMGs are rare examples of extreme starburst galaxies with star formation rates (SFRs) of $\gtrsim 1000$ M$_\odot$ yr^{-1} and therefore are not representative of the general population of dusty star-forming galaxies. Consequently, our understanding of the nature of these sources, at the earliest epochs, is still incomplete. Here we report the spectroscopic identification of a gravitationally amplified ($\mu = 9.3 \pm 1.0$) dusty star-forming galaxy at $z = 6.027$. After correcting for gravitational lensing we derive an intrinsic SFR of 380 ± 50 M$_\odot$ yr^{-1} for this source, and find that its gas and dust properties are similar to those measured for local Ultra Luminous Infrared Galaxies (ULIRGs), extending the local trends up to an unexplored territory at high redshift. This ULIRG-like galaxy at $z = 6$ suggests a universal star-formation efficiency during the last 12.8 Gyr for dusty star-forming galaxies.

HATLAS J090045.4+004125 ($\alpha = 09^{\rm h}00^{\rm m}45.8$, $\delta = +00^\circ41'23''$; hereafter G09 83808, since it was detected in the GAMA 09hrs field) is part of a sub-sample of the *Herschel* ATLAS '500 μm-riser' galaxies[14] with ultra-red far-infrared (FIR) colours of $S_{500_{\mu{\rm m}}}/S_{250_{\mu{\rm m}}} > 2$ and $S_{500_{\mu{\rm m}}}/S_{350_{\mu{\rm m}}} > 1$, with a flux density threshold of $S_{500_{\mu m}} < 80$ mJy. The FIR colours of this source are consistent with thermal dust emission redshifted to $z > 4$ and represent a relatively simple selection criterium to find high-redshift galaxies. A similar selection allowed the identification of HFLS3[12], an extreme starburst galaxy (even after corrected for gravitational amplification[15]) at $z = 6.3$, in the HerMES blank field survey[3].

G09 83808 was observed, among other ultrared-*Herschel* dusty star-forming galaxies, as part of a follow-up program with the Large Millimeter Telescope *Alfonso Serrano* (LMT) using the AzTEC camera, in order to obtain higher angular resolution ($\sim$ 8.5 arcsec) continuum observations at 1.1 mm. A sub-sample of those galaxies detected as a single source in the AzTEC images (i.e. with no evidence of multiple components) and with photometric redshifts of > 4, was selected for spectroscopic observations in the 3 mm band using the Redshift Search Receiver (RSR) on the LMT. In the LMT/RSR spectrum of G09 83808 we identify three emission lines corresponding to ^{12}CO($6-5$), ^{12}CO($5-4$), and $H_2O(2_{11} - 2_{02})$ (see Fig. 1). Based on these lines we unambiguously determine the galaxy redshift to be $z = 6.0269 \pm 0.0006$ (i.e. when the Universe was just 900 million years old). Follow-up observations with the SMA telescope confirm this solution through the detection of the redshifted [CII] ionized carbon line at 270.35 GHz (Fig. 1).

High-angular resolution observations ($0.24\ \mathrm{arcsec} \times 0.13\ \mathrm{arcsec}$, corresponding to a physical scale of $\sim$ 1 kpc at this redshift) taken with the Atacama Large Millimeter/submillimeter Array (ALMA) at $\sim 890\ \mu\mathrm{m}$ reveal a double arc structure (in a partial Einstein ring configuration of radius $\sim$ 1.4 arcsec) around a foreground galaxy at $z = 0.776$ (see Fig. 2), implying strong gravitational amplification of the high-redshift background galaxy. Using these ALMA continuum observations to constrain the effects of gravitational lensing, modelling directly the visibilities in the *uv* plane (see Methods section for additional details), we derive a gravitational amplification factor of $\mu = 9.3 \pm 1.0$. This amplification factor is used to derive the intrinsic physical properties of G09 83808.

Using the *Herschel* 250, 350, and 500 μm photometry[14], combined with the SCUBA-2 850 μm[14] imaging and our AzTEC 1.1 mm observations (see Table 1), we model the continuum spectral energy distribution (SED; see Figure 3). We estimate an infrared (IR, $8-1000\ \mu$m) luminosity, $L_{\rm IR}$, of $3.8 \pm 0.5 \times 10^{12}$ $L_\odot$ (corrected for gravitational magnification) which implies a SFR[a] of $380 \pm 50\ \mathrm{M_\odot yr^{-1}}$ (see Methods section for more information). This implies that G09 83808 is a member of the Ultra Luminous Infrared Galaxy (ULIRGs[16]) population. This is the only SMG with an unambiguous spectroscopic redshift in this luminosity range at $z \gtrsim 5$, lying between the extreme obscured starbursts[7–9,12,13] ($\gtrsim 1000$ $M_\odot$ yr^{-1}) discovered at submm wavelengths and the UV/optical selected star-forming galaxies with follow-up detections at submm wavelengths[17–19] ($\lesssim 100$ $M_\odot$ yr^{-1}).

Although these galaxies are unreachable with the current generation of submm wide-area surveys[3,4] without the benefit of gravitational amplification, they can be found in the deepest surveys recently achieved with ground-based telescopes, such as the James Clerk Maxwell Telescope (JCMT) SCUBA-2 Cosmology Legacy Survey (S2CLS). However, none of them has yet been spectroscopically confirmed. With the caveat of using the position of the dust SED peak as an estimation of redshift, a study based on S2CLS observations[5] has derived a comoving space density of $3.2 \times 10^{-6}\ \mathrm{Mpc^{-3}}$ for sources with $300 < \mathrm{SFR} < 1000\ \mathrm{M_\odot\ yr^{-1}}$ at $5 < z \lesssim 6$ (i.e. in the range probed by our galaxy). With a duty-cycle correction of ≈ 40 Myr, as the gas depletion time scale measured for G09 83808 (see below) and other galaxies[12], we estimate the corrected comoving space density of this population of galaxies to be $\approx 2 \times 10^{-5}\ \mathrm{Mpc^{-3}}$, which perfectly matches that of massive quiescent galaxies at $z \approx 3-4$ (refs.[20]). This suggests, that these ULIRG-type galaxies at $5 \lesssim z \lesssim 6$ are the progenitors of these quiescent

[a]Here we will use SFR to refer to the dust-obscured SFR

galaxies, which cannot be explained only by the rare extreme starburst (like HFLS3), since they are an order of magnitude less abundant[14].

Based on the CO lines detected in the LMT/RSR spectrum we derive a molecular gas mass of $\mathrm{M(H_2)} = 1.6 \pm 0.6 \times 10^{10}$ $\mathrm{M_\odot}$ (see Methods section for details). This implies a gas depletion timescale of $\mathrm{M(H_2)/SFR} \approx 40$ Myr, consistent with the value found for other SMGs at lower redshifts with ULIRG-luminosity[22]. G09 83808 shows a remarkable large gas mass fraction of $f_{\rm gas} = M_{\rm H_2}/M_{\rm dyn} \sim 60\%$ (see Methods secction), among the largest measured for star forming galaxies at $z \approx 2-3$ (ref. [21]). The CO(6-5)/CO(5-4) line luminosity ratio of 0.4 ± 0.1 is in agreement with local ULIRGs (although lower than the average[24]), and implies a CO ladder peaking at J≤ 5 (i.e. less excited than AGN-dominated galaxies[23]). These two CO transitions, as well as the H_2O line, lie (within the error bars) on their respective FIR/IR-line luminosity relations ($L_{\rm FIR} \propto L_{\rm CO(6-5)}^{0.93}$, $L_{\rm FIR} \propto L_{\rm CO(5-4)}^{0.97}$, and $L_{\rm H_2O} \propto L_{\rm IR}^{1.16}$) found for local ULIRGs and lower redshifts SMGs[24,25]. The star-formation efficiency (SFE) of our galaxy, estimated through the $L'_{CO} - L_{\rm IR}$ relation (which describes the relationship between the luminosity due to star formation and the gas content), is similar to local (U)LIRGs (see Fig. 4). This suggests a universal SFE across several decades of molecular gas masses from $z = 6$ to $z \sim 0$ (i.e., during the last 12.8 Gyr of the Universe) for this kind of galaxies (although some works[26] have reported a slight evolution of the SFE with redshift). In addition, the estimated dust mass of $M_d = 1.9 \pm 0.4 \times 10^8$ $\mathrm{M_\odot}$ results in a gas-to-dust ratio, $\delta_{\rm GDR}$, of 80 ± 30. This is in agreement with the value estimated for HFLS3[12] and also with local (U)LIRGs[27] ($\delta_{\rm GDR} = 120 \pm 28$).

The luminosity of the [CII] ionized carbon line detected with the SMA is $1.3 \pm 0.4 \times 10^9$ $\mathrm{L_\odot}$ which corresponds to a [CII]/FIR ratio of $3.4 \pm 1.1 \times 10^{-4}$, a value that is among the lowest measured for local (U)LIRGs and SMGs. As shown in Figure 4, our source follows the same [CII] deficiency trend measured for local LIRGS[28] extending it to $\mathrm{L_{FIR}} \gtrsim 10^{12}$ $\mathrm{L_\odot}$ and up to $z = 6$. The [CII]/FIR ratio of G09 83808 is also consistent with the lowest values measured for lower-redshift SMGs and lies on a region where SMGs and AGN-host galaxies converge (Fig. 4). It may be the case that other SMGs suffer from gravitiational amplification, which could help to reduce the large scatter since many of these galaxies should fall along the LIRG relation when corrected for magnification. However, the intrinsic scatter in the relation is high[28], even for the local sample, and therefore, larger samples of SMGs are required to derive conclusions about the origin of the [CII] deficiency.

We confirm the existence of ULIRG-like galaxies within the first billion years of Universe's history. These sources may be more representative of the dusty star-forming galaxy population at these epochs than the extreme starbursts previously discovered. Four emission-line-selected galaxies with similar luminosities and redshifts have been recently found around quasars[29] (with the caveat of using just one line for redshift determination), however, the properties of these sources may be affected by the companion quasar and therefore not representative of the whole population. Although G09 83808 shows similar properties to those measured in lower-redshift SMGs, its higher dust temperature ($T_d = 49 \pm 3$ K) and compact morphology ($R_{1/2} = 0.6 \pm 0.1$ kpc) resemble that of local ULIRGs. For comparison, typical UV/optically-selected star-forming galaxies at $z \sim 6$ have SFRs ~ 10 times lower and radii ~ 1.7 times larger than G09 83808[30]. This study is hence crucial for understanding the evolutionary path of SMGs and their link with local galaxies. Although a larger sample is needed to statistically estimate the properties of these sources and their contribution to the cosmic star formation history, this galaxy suggests that star formation in dusty star-forming galaxies has been driven by similar physical processes during the last ~ 12.8 Gyr .

Acknowledgements We thank Ian Smail for insightful comments that has improved the quality of the paper. JAZ acknowledges support from a mexican CONACyT studentship. RJI, LD and IO acknowledge support from ERC in the form of the Advanced Investigator Programme, 321302, COSMICISM. LD additionally acknowledges support from the ERC Consolidator Grant CosmicDust. HD acknowledges financial support from the Spanish Ministry of Economy and Competitiveness (MINECO) under the 2014 Ramón y Cajal program MINECO RYC-2014-15686. MJM acknowledges the support of the National Science Centre, Poland through the POLONEZ grant 2015/19/P/ST9/04010 and the European Union's Horizon 2020 research and innovation programme under the Marie Skłodowska-Curie grant agreement No. 665778. This work would not have been possible without the long-term financial support from the Mexican CONACyT during the construction and early operational phase of the Large Millimeter Telescope *Alfonso Serrano*, as well as support from the US National Science Foundation via the University Radio Observatory program, the Instituto Nacional de Astrofísica, Óptica y Electrónica (INAOE), and the University of Massachusetts (UMass). The Submillimeter Array is a joint project between the Smithsonian Astrophysical Observatory and the Academia Sinica Institute of Astronomy and Astrophysics and is funded by the Smithsonian Institution and the Academia Sinica.

Author Contributions JAZ led the scientific analysis and the writing of the paper, as well as the SMA follow-up proposal. RJI, EV, SE, AC, HD, JSD, LD, MJM, SS, IS, MWLS, and PW have contributed to the original *Herschel* proposals and source selection of the red sources, where this source was originally identify. AM, DHH, EV, IA, VAR, MC, DRG, ET, and OV performed the selection of the sample for the LMT observations and lead the LMT proposals. MSY, GN, DS, GW, DSA, AV, and MZ carried out LMT data reduction and interpretation. DW, MY, and AIGR assisted with the SMA observations and data reduction. JS, IO, HN have contributed to the data analysis and to fitting and modeling the results. All the authors have discussed and contributed to this manuscript.

Competing Interests The authors declare that they have no competing financial interests.

Correspondence Correspondence and requests for materials should be addressed to JAZ (email: zavala@inaoep.mx).

REFERENCES

1. Smail, I. *et. al.* A Deep Sub-millimeter Survey of Lensing Clusters: A New Window on Galaxy Formation and Evolution. *Astrophys. J. Lett.* **490** L5-L8 (1997).
2. Hughes, D. *et. al.* High-redshift star formation in the Hubble Deep Field revealed by a submillimetre-wavelength survey. *Nature* **394**, 241-247 (1998).
3. Oliver S. *et. al.* The Herschel Multi-tiered Extragalactic Survey: HerMES. *Mon. Not. R. Astron. Soc.* **424**, 1614-1635 (2012).
4. Valiante E. *et. al.* The Herschel-ATLAS data release 1 - I. Maps, catalogues and number counts. *Mon. Not. R. Astron. Soc.* **462**, 3146-3179 (2016).
5. Michałowski, M. *et. al.* The SCUBA-2 Cosmology Legacy Survey: the nature of bright submm galaxies from 2 deg2 of 850-um imaging. *Mon. Not. R. Astron. Soc.;* arXiv preprint: 1610.02409 (2017).
6. Blain, A. & Longair, M. Submillimetre cosmology. *Mon. Not. R. Astron. Soc.* **264**, 509-521 (1993).
7. Capak, P. *et. al.* A massive protocluster of galaxies at a redshift of $z \sim 5.3$. *Nature* **470** 233-235 (2011).
8. Combes, F. *et. al.* A bright z = 5.2 lensed submillimeter galaxy in the field of Abell 773. HLSJ091828.6+514223. *Astron. Astrophys. Lett.* **538**, L4 (2012).
9. Walter, F. *et. al.* The intense starburst HDF850.1 in a galaxy overdensity at z=5.2 in the Hubble Deep Field. *Nature* **486**, 233-236 (2012).
10. Ma, J. *et. al.* Stellar Masses and Star Formation Rates of Lensed, Dusty, Star-forming Galaxies from the SPT Survey. *Astrophys. J.* **812**, 88-104 (2015).
11. Riechers, D. *et. al.* Rise of the Titans: A Dusty, Hyper-Luminous '870 micron riser' Galaxy at z˜6. *Astrophys. J.* arXiv preprint: 1705.09660 (2017).
12. Riechers, D. *et. al.* A Dust-Obscured Massive Maximum-Starburst Galaxy at a Redshift of 6.34. *Nature* **496**, 329-333 (2013).
13. Strandet, M. *et. al.* ISM properties of a Massive Dusty Star-Forming Galaxy discovered at z ˜ 7. *Astrophys. J. Lett.* arXiv preprint: 1705.07912 (2017).
14. Ivison, R. *et. al.* The Space Density of Luminous Dusty Star-forming Galaxies at $z > 4$: SCUBA-2 and LABOCA Imaging of Ultrared Galaxies from Herschel-ATLAS. *Astrophys. J.* **832**, 78- (2016).
15. Cooray, A. *et. al.* HerMES: The Rest-frame UV Emission and a Lensing Model for the z = 6.34 Luminous Dusty Starburst Galaxy HFLS3. *Astrophys. J.* **790**, 40- (2014).
16. Sanders, D & Mirabel, I. Luminous Infrared Galaxies. *Ann. Rev. Astron. Astrophys.* **34**, 749- (1996).

17. Capak, P. *et. al.* Galaxies at redshifts 5 to 6 with systematically low dust content and high [C II] emission *Nature* **522** 455-458 (2015).
18. Watson, D. *et. al.* A dusty, normal galaxy in the epoch of reionization. *Nature.* **519**, 327-330 (2015).
19. Willott, C., Carilli, C., Wagg, J. & Wang, R. Star Formation and the interstellar medium in $z > 6$ UV-luminous Lyman-break galaxies. *Astrophys. J.* **807**, 180- (2015).
20. Straatman, C. *et. al.* The Sizes of Massive Quiescent and Star-forming Galaxies at $z \sim 4$ with ZFOURGE and CANDELS. *Astrophys. J. Lett.* **808**, L29- (2015).
21. Tacconi, L. *et. al.* High molecular gas fractions in normal massive star forming galaxies in the young Universe. *Nature.* **463**, 781-784 (2010).
22. Bothwell, M. *et. al.* A survey of molecular gas in luminous sub-millimetre galaxies. *Mon. Not. R. Astron. Soc.* **429**, 3047-3067 (2013).
23. Carilli, C. & Walter, F. Cool Gas in High-Redshift Galaxies. *Ann. Rev. Astron. Astrophys.* **51**, 105-161 (2013).
24. Greve, T. *et. al.* Star Formation Relations and CO Spectral Line Energy Distributions across the J-ladder and Redshift. *Astrophys. J.* **794**, 142- (2014).
25. Yang, C. *et. al.* Submillimeter H_2O and H_2O^+emission in lensed ultra- and hyper-luminous infrared galaxies at $z = 2 - 4$. *Astron. Astrophys.* **595**, 80- (2016).
26. Scoville, N. *et. al.* Evolution of Interstellar Medium, Star Formation, and Accretion at High Redshift. *Astrophys. J.* **837**, 150- (2017).
27. Wilson, C. *et. al.* Luminous Infrared Galaxies with the Submillimeter Array. I. Survey Overview and the Central Gas to Dust Ratio. *Astrophys. J. Suppl. Ser.* **178**, 189-224 (2008).
28. Díaz-Santos, T. *et. al.* Explaining the [C II]157.7 μm Deficit in Luminous Infrared Galaxies - First Results from a Herschel/PACS Study of the GOALS Sample. *Astrophys. J.* **774**, 68- (2013).
29. Decarli, R. *et al.* Rapidly star-forming galaxies adjacent to quasars at redshifts exceeding 6. *Nature*. arXiv preprint:1705.08662 (2017).
30. Rodriguez-Puebla, A, Primack, J., Avila-Reese, V. & Faber, S. Constraining the galaxy-halo connection over the last 13.3 Gyr: star formation histories, galaxy mergers and structural properties. *Mon. Not. R. Astron. Soc.* arXiv preprint:1703.04542 (2017).

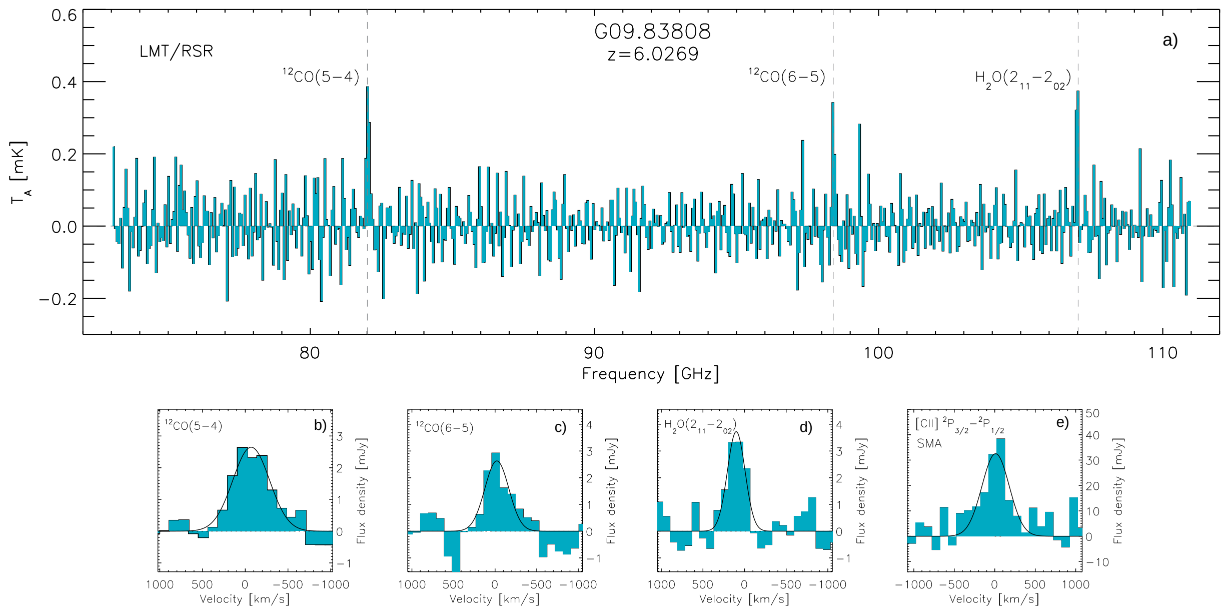

Figure 1: Identification of molecular emission lines and redshift derivation. a), Wide-band Redshift Search Receiver (RSR) 3 mm spectrum of G09 83808 taken with the Large Millimeter Telescope (LMT). The transitions detected above $\mathrm{S/N} = 5$ are marked with vertical dashed lines, and correspond to ^{12}CO(5-4), ^{12}CO(6-5), and $H_2O(2_{11} - 2_{02})$ at $z = 6.0269 \pm 0.0006$. The spectrum has been rebinned into 2 pixels bins ($\sim 200\mathrm{km/s}$) for better visualization. **b), c), d),** LMT/RSR raw spectra at the position of the detected lines along with the best-fitting Gaussian profiles. **e),** SMA spectrum centered at the position of the detected line. The x-axes is in velocity offset with respect to the derived redshift of $z = 6.0269$. The derived properties of the lines are reported in Table 1.

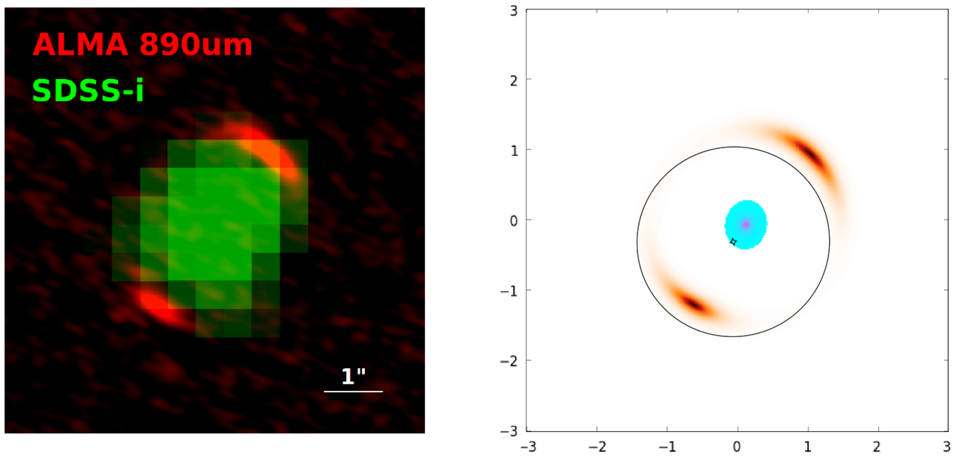

Figure 2: **ALMA high-angular resolution continuum observations and lensing model.** *Left:* Color composite image of G09 83808. The green channel represents the i-band data from SDSS and the red channel the ALMA 890 μm observations. An Einstein ring-like structure of radius ≈ 1.4 arcsec in the ALMA image is clearly seen around a foreground galaxy at $z = 0.776$, which confirms that our high-redshift galaxy is strongly amplified. *Right:* Best-fit lensing model based on the visibilities of ALMA observations, from which we derived a gravitational amplification of $\mu = 9.3 \pm 1.0$.

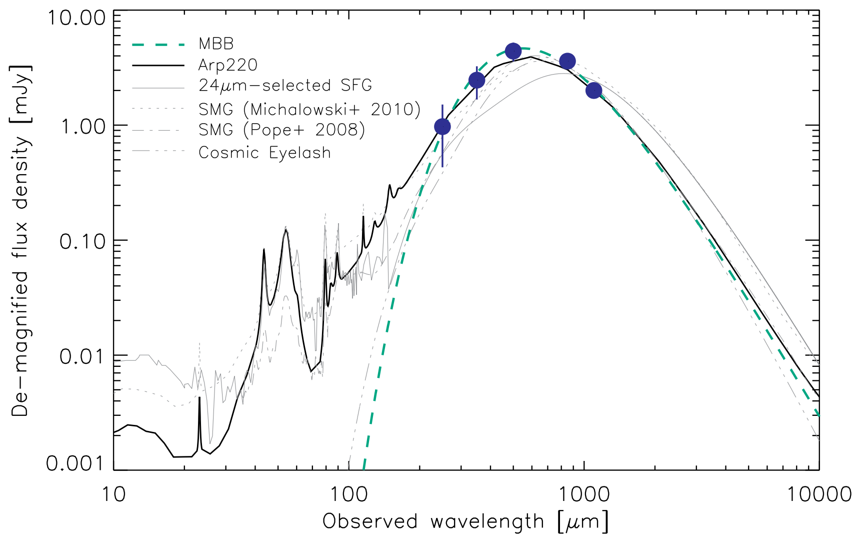

Figure 3: Photometry and spectral energy distribution (SED). De-magnified (with $\mu = 9.3 \pm 1.0$) flux densities at 250, 350, 500, 850 and 1100 μm from *Herschel/SPIRE*, JCMT/SCUBA-2, and AzTEC/LMT are represented by the blue circles. These flux densities were fitted with different SED templates, including: Arp220, Cosmic Eyelash, two average SMG templates, an average 24 μm-selected star-forming galaxy template, and a modified black body (MBB, see Methods section for details). We achieve the lowest χ^2 with the Arp220 template, from which we derive an IR luminosity of $3.8 \pm 0.5 \times 10^{12}$ (corrected for magnification). From the best-fit modified black body distribution we derive a dust temperature of 49 ± 3 K. As discussed in the Methods section, the CMB effects are not significant.

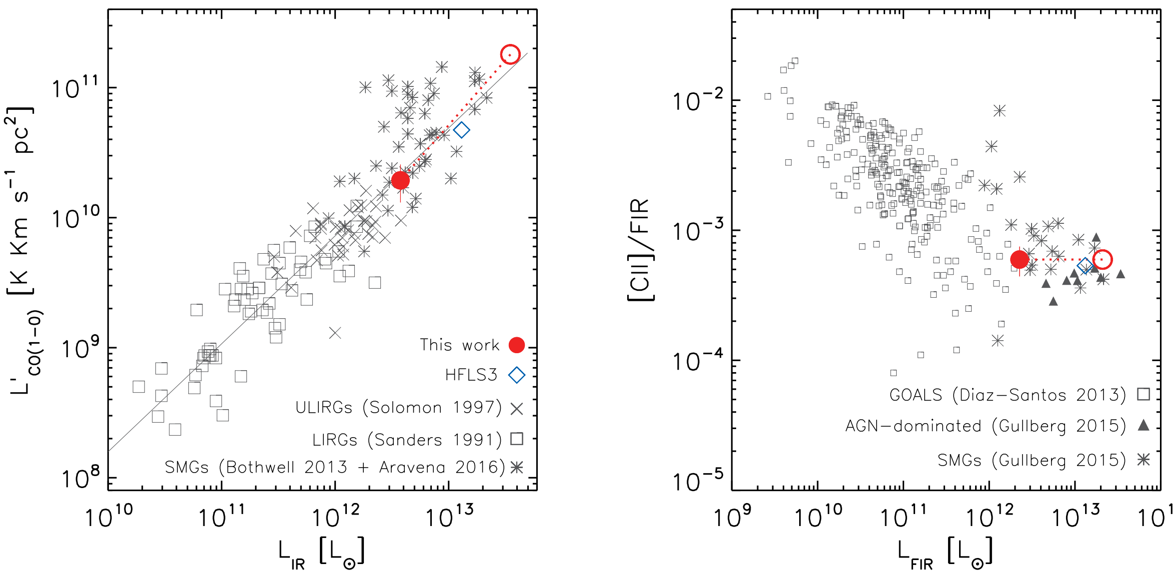

Figure 4: Star formation efficiency and [CII] deficiency. *Left:* Lens-corrected CO(1-0) luminosity versus IR luminosity ($L'_{\rm CO(1-0)} - L_{\rm IR}$) as a proxy for the star-formation efficiency of G09 83808. For comparison, local LIRGS[31], ULIRGS[32], and lower-redshift SMGs[22,33] are plotted along with the best-fit relation to the three samples[22]. As can be seen, G09 83808 falls on the same relation (as well as HFLS3[12] after correcting for magnification[15]), which suggests that the same star formation efficiency holds from $z \sim 0$ to $z = 6$ (i.e. during the last ~ 12.8 Gyr). The empty circle represents the position of our source if no lensing amplification correction is applied. *Right:* [CII]/FIR versus de-magnified (filled circle) and amplified (empty circle) FIR luminosity for G09 83808. For comparison, we also plot a sample of (U)LIRG galaxies from the Great Observatories All-sky Survey (GOALS[28]), and a compilation of high-redshift sources[45] that includes SMGs and AGN-dominated sources. Our source follows the same trend as local (U)LIRGs and lies in a region between lower-redshift SMGs and AGNs.

Table 1: **Measured spectral line and continuum properties (not corrected for gravitational amplification).**

	Transition				Photometry[a]	
	CO(5-4)	CO(6-5)	$H_2O(2_{11} - 2_{02})$	[CII]	[μm]	[mJy]
$\nu_{\rm obs}$ [GHz]	82.031 ± 0.007	98.41 ± 0.01	106.993 ± 0.007	270.35 ± 0.03	250	9.7 ± 5.4
FWHM [km s^{-1}]	490 ± 60	320 ± 70	240 ± 40	400 ± 70	350	24.6 ± 7.9
$S_{\rm int}$ [Jy km s^{-1}]	1.6 ± 0.3	0.9 ± 0.3	0.8 ± 0.2	13.8 ± 3.0	500	44.0 ± 8.2
L' [10^{10} K km s^{-1} pc^{-2}]	7.6 ± 1.2	2.9 ± 0.8	2.3 ± 0.5	6.1 ± 1.3	850	36.0 ± 3.1
					1100	20.0 ± 1.0

[a]The flux densities at 250, 350, 500, and 850 μm were taken from ref.[14]

Methods

1 Observations and data reduction

1.1 LMT observations

Continuum and spectroscopic observations were obtained using the Large Millimeter Telescope (LMT[34], PI: D. Hughes), located on the summit of Volcán Sierra Negra (*Tliltépetl*), Mexico, at ~ 4600 m.a.s.l. Observations were carried out during the Early Science Phase of the telescope using the 1.1 mm continuum camera, AzTEC[35], and the 3 mm spectrograph, Redshift Search Receiver (RSR[36]). During these observations only the inner 32-m diameter region of the telescope active surface was illuminated, which provided an effective beam size of ≈ 8.5 arcsec at 1.1 mm and between $20 - 28$ arcsec in the RSR 3 mm window (75 GHz - 110 GHz).

AzTEC observations were performed on 2014 November 10 with an opacity of $\tau_{225} = 0.07$ and total on-source integration time of 11 min. Data reduction were done following the AzTEC Standard Pipeline[37]. G09 83808 was detected with a S/N ≈ 20 with a flux density of $S_{1.1\mathrm{mm}} = 20.0 \pm 1.0$ mJy. RSR observations were subsequently taken at the AzTEC position in two different periods: February 2016 and February 2017, along five different nights with an opacity range of $\tau_{225} = 0.05 - 0.15$ and a total integration time of 8 hrs. Pointing observations on bright millimetre sources were done every hour. Data reduction was performed using the Data Reduction and Analysis Methods in Python (DREAMPY). The final spectra were obtained by averaging all scans using $1/\sigma^2$ weights after flagging bad data. Finally, to convert from antenna temperature units to flux, a factor of 7 Jy K^{-1} was used[38]. The final spectrum shows three lines detected at S/N $\gtrsim 5$ associated to CO(6-5), CO(5-4) and $H_2O(2_{11} - 2_{02})$ at $z = 6.0269$. A cross-correlation template analysis[38] also identifies this redshift as the best solution with a S/N $= 9.1$. Figure 1 shows the final spectrum after a Savitzky-Golay filter[39] has been applied for better visualization (the filter does not modified any of the properties of the detected lines).

At the redshift of our source the [CII] 158 μm line (see below) falls within the AzTEC band pass and then contributes to the total flux density measured at 1.1 mm. However, the contamination from the line is measured to be less than 2 per cent. Even if the [CII] line luminosity was as high as 1 per cent of the total IR luminosity, the contamination to the AzTEC measurement would be only ~ 6 per cent, which is similar to the absolute flux calibration uncertainty. Therefore, and at least for this source, the contamination of the emission line to the 1.1 mm continuum flux density is less important than anticipated[40].

1.2 SMA observations

G09 83808 was observed with the Submillimeter Array (SMA, PI: J. Zavala) on Mauna Kea, Hawaii, on 2017 April 03. The weather conditions were good, with an average atmospheric opacity of $\tau_{225} = 0.07$ and stable phase. The seven available array antennas were in a compact configuration that provided baseline lengths from 8 to 77 meters. The '345' receiver set was tuned to provide spectral coverage $\pm(4 - 12)$ GHz from a LO frequency of 277.5 GHz, specifically to span a broad range around the estimated (redshifted) [CII] line frequency of ~ 270.5 GHz in the lower sideband. The SWARM correlator provided uniform channel spacing of 140 kHz ($\sim$0.16 km s^{-1}) over the full bandwidth. The usable field of view is set by the FWHM primary beam size of ~ 47 arcsec at this frequency.

The basic observing sequence consisted of a loop of 2 minutes each on the gain calibrators J0909+013 (1.57 Jy) and J0831+044 (0.47 Jy) and 17.5 minutes on G09 83808. The track spanned an hour angle range of -0.8 to 4.8 for the target source. Passband calibration was obtained with observations of the strong quasar 3C279. The absolute flux scale was set using observations of Callisto, with an estimated accuracy of 20%. All of the basic calibration steps were performed using standard procedures in the MIR software package. The calibrated visibilities were exported to the MIRIAD software package for imaging and deconvolution. Within MIRIAD, the task `uvaver` was used to combine the 4 correlator windows of the lower sideband and to resample the visibilities to 50 km s^{-1} spectral resolution. The task `uvlin` was used for continuum subtraction, using a linear fit to line-free channel ranges in the band. The task `invert` provided Fourier inversion for both continuum and spectral line imaging, followed by `clean` for deconvolution. The synthesized beam size obtained with natural weighting was $2.5'' \times 2.3''$, p.a. 82° for the spectral line data cube, with rms noise 7.1 mJy per 50 km s^{-1} bin. The final spectrum (see Fig. 1) was then extracted from a rectangular region that comprise all the continuum emission. We measured the continuum flux density of the source to be 21.5 ± 3 mJy, in very good agreement with the AzTEC photometry.

2 Lensing model

The lens model was created using the publicly-available `visilens` code[41]; details of the code are given in that work. Briefly, the lens mass profile is parameterized as a Singular Isothermal Ellipsoid, and the background source is modeled with a single elliptical Sérsic profile. The parameter space is explored using a Markov Chain Monte Carlo sampling method, generating a model lensed image at each proposed combination of lens and source parameters. The redshift of both sources is fixed at $z = 0.776$ (based on X-Shooter/VLT observations[42]) and $z = 6.027$, respectively. Because pixel values in interferometric images are correlated and subject to difficult-to-model residual calibration errors, the proposed model image is inverted to the visibility domain and sampled at the uv coordinates of the ALMA data (Project code: 2013.1.00001.S; PI: R. Ivison; Oteo et al. in preparation). We also allow for residual antenna-based phase calibration errors in the model which could be due to, for example, uncompensated atmospheric delays. The phase shifts of all antennas are < 10 deg, indicating that no significant antenna-based calibration problems remain.

The lensed emission is reasonably well-fit by a single background Sérsic component, leaving peak residuals of $\sim 4\sigma$ (the source is detected at peak significance $\sim 20\sigma$). These residuals may indicate that either the lens, source, or both are more complex than the simple parametric forms we have assumed. We have verified that an additional background source component is not statistically motivated. The best-fit magnification of the source is $\mu_{890\mu\mathrm{m}} = 9.3 \pm 1.0$, with an intrinsic flux density $S_{890\ \mu\mathrm{m}} = 4.3 \pm 0.5$ mJy and half-light radius 0.10 ± 0.01" ($= 0.6 \pm 0.1$ kpc). This compact morphology resembles the sizes found for local ULIRGs[43] ($\sim$ 0.5 kpc), which are smaller than the typical values in SMGs ($\sim$ 1.8 kpc, ref:[44]).

3 SED fitting and dust properties

We fit different galaxy SED templates to the photometry of G09 83808 through a χ^2 minimization method. We include the SED template of Arp220[46], Cosmic Eyelash[47] (SMM J2135-0102), two average SMGs templates[48,49], and finally a composite SED of 24 μm-selected star-forming galaxy[50]. All the SED templates were fixed at $z = 6.027$. The Arp220 SED template gives us the best fit with $\chi^2_{\mathrm{red}} = 0.7$. Using this template we derive an IR $(8 - 1000\mu\mathrm{m})$ luminosity of $3.8 \pm 0.5 \times 10^{12}$ L$_\odot$ and a FIR $(42.5 - 122.5\mu\mathrm{m})$ luminosity of $2.3 \pm 0.3 \times 10^{12}$ L$_\odot$ (both corrected for gravitational amplification) . For comparison, if we adopt instead a SMGs average template ($\chi^2_{\mathrm{red}} = 1.2$) we obtain $\mathrm{L_{IR}} = 3.0 \pm 0.4 \times 10^{12}$ L$_\odot$, which is in good agreement with the value derived using the Arp220 template. Using Kennicutt standard relation[51] for a Chabrier initial mass function (IMF)[53], this IR luminosity corresponds to a star formation rate (SFR) of 380 ± 50 M$_\odot$ yr^{-1}, or to 570 ± 70 M$_\odot$ yr^{-1} if the most recent relation[52] is used. If we adopt instead the Kennicutt calibration[51] for a Salpeter IMF[54], the SFR increases to 640 ± 90 M$_\odot$ yr^{-1}, still below the range probed by other SMGs at $z \gtrsim 5$.

We also use a modified blackbody function to fit our photometric measurements described by

$$S_\nu \propto \{1 - \exp[-(\nu/\nu_0)^\beta]\} B(\nu, T_\mathrm{d}), \qquad (1)$$

where S_ν is the flux density at frequency ν, ν_0 is the rest-frame frequency at which the emission becomes optically thick, T_d is the dust temperature, β is the emissivity index, and $B(\nu, T_\mathrm{d})$ is the Planck function at temperature T_d. To minimize the number of free parameters, the emissivity index is fixed (previous observational works suggest $\beta = 1.5-2$; refs.[55–57]), as well as $\nu_0 = c/100\ \mu$m (refs.[12,58]), where c is the speed of light. From the best fit ($\chi^2 \approx 1.1$) we derive $T_d = 49 \pm 3$ K for $\beta = 1.8$ and $T_d = 52 \pm 3$ K for $\beta = 1.5$. For these dust temperatures and at the redshift of our source the CMB effects[59] are not significant ($\Delta T \lesssim 1$ K).

Assuming the dust is isothermal, the dust mass, M_d, is estimated from

$$M_\mathrm{d} = \frac{S_{\nu/(1+z)} D_L^2}{(1+z)\kappa_\nu B(\nu, T_\mathrm{d})}, \quad (2)$$

where S_ν is the flux density at frequency ν, κ_ν is the dust mass absorption coefficient at ν, T_d is the dust temperature, and $B(\nu, T_d)$ is the Planck function at temperature T_d. The dust mass absorption follows the same power law as the optical depth, $\kappa \propto \nu^\beta$. Assuming normalization of $\kappa_\mathrm{d}(850\mu\mathrm{m}) = 0.07$ m^2 kg^{-1} (ref.[60]) and a dust temperature of 49 ± 3 K, we estimate a dust mass of $\mathrm{M_d} = 1.9 \pm 0.4 \times 10^8\ \mathrm{M_\odot}$ after correcting for the CMB effects[59] (although this correction is less than 5 per cent). These calculations do not include the uncertainties of the dust mass absorption coefficient, which could be at least a factor of 3 (ref. [61]). If we use instead a lower dust temperature of 35 K, the dust mass increases by a factor of ~ 2.

We also fit the observerd photometry with the MAGPHYS[62] SED modelling code finding consistent results, within the error bars, with median values of SFR= $360^{+80}_{-70}\ \mathrm{M_\odot\ yr^{-1}}$, $\mathrm{L_{IR}} = 4.5 \pm 0.7 \times 10^{12}\ \mathrm{L_\odot}$, $T_d = 40^{+4}_{-2}$ K, and $\mathrm{M_d} = 4.2 \pm 0.7 \times 10^8\ \mathrm{M_\odot}$.

4 Spectral line properties

We calculate the line luminosity for each detected line following the standard relation[63] described by:

$$L'_\mathrm{CO} = 3.25 \times 10^7 S_{CO}\Delta V\ \nu_{obs}^{-2}\ D_L^2\ (1+z)^{-3}, \quad (3)$$

where L'_CO is the line luminosity in K km s^{-1} pc^2, $S_{CO}\Delta V$ is the velocity-integrated line flux in Jy km s^{-1}, ν_{obs} is the observed central frequency of the line in GHz and D_L is the luminosity distance in Mpc. The integrated flux, $S_{CO}\Delta V$, is calculated as the integral of the best-fit Gaussian distribution, and its associated uncertainty through Monte Carlo simulations taking into account the errors in the Gaussian parameters (i.e. peak flux density and line width). To estimate the line luminosity in $\mathrm{L_\odot}$, we use $L = 3 \times 10^{-11} \nu_r^3 L'$, where ν_r is the rest frequency of the line[63]. All properties are summarized in Table 1.

5 CO(1-0) line luminosity and molecular gas mass

The molecular gas mass, $\mathrm{M(H_2)}$, can be derived using the CO luminosity to molecular gas mass conversion factor, α, following the relation

$$\mathrm{M(H_2)} = \alpha\ \mathrm{L'_{CO(1-0)}}. \quad (4)$$

For the $\mathrm{L'_{CO(1-0)}}$ line luminosity we adopt the average value of $\mathrm{L'_{CO(1-0)}} = 2.0 \pm 0.8 \times 10^{10}$ K km s^{-1} pc^{-2} extrapolated from our CO(6-5) and CO(5-4) transitions and correcting for gravitational amplification. The extrapolation was done using average brightness ratios found for lower-redshift SMGs[22] ($\mathrm{L'_{CO(5-4)}/L'_{CO(1-0)}} = 0.32 \pm 0.05$, $\mathrm{L'_{CO(6-5)}/L'_{CO(1-0)}} = 0.21 \pm 0.04$), this sample includes galaxies with similar luminosities to G09 83808 and are in agreement with those found for local ULIRGs[24] (within the large scatter). On the other hand, if we use the relationship between the Rayleigh-Jeans specific luminosity and CO(1-0) luminosity[64], $\mathrm{L'_{CO(1-0)}}$ [K km s^{-1}pc^2] $= 3.02 \times 10^{-21} \mathrm{L_\nu}$ [erg s^{-1} Hz^{-1}], we obtain a consistent line luminosity of $1 \pm 0.1 \times 10^{10}$ K km s^{-1} pc^{-2} (assuming a mass-weighted dust temperature of 35 K, which is different from the luminosity-weighted dust temperature determined from the SED fitting[64]). Using the former value and $\alpha = 0.8\ \mathrm{M_\odot}$ (K km s^{-1} pc^{-2})$^{-1}$, which is appropriate for starburst galaxies[23] (although some studies suggest larger values[65]), we derive a molecular mass of $\mathrm{M(H_2)} = 1.6 \pm 0.6 \times 10^{10}\ \mathrm{M_\odot}$.

6 Dynamical mass and gas mass fraction

Dynamical mass has been derived using the 'isotropic virial estimator', which has been shown to be appropriate for lower-redshift SMGs[66]:

$$M_{\rm dyn}[M_\odot] = 2.8{\times}10^5\ \Delta\nu^2_{\rm FWHM}[{\rm km\ s^{-1}}]\ R_{1/2}[{\rm kpc}], \quad (5)$$

where $\Delta\nu_{\rm FWHM}$ is the integrated line FWHM, which has been assumed to be 400 km/s (as the average between the CO and [CII] lines), and $R_{1/2}$ is the half-light radius of $\sim$ 0.6 kpc (derived from the lesing model of the continuum emission). This results in a dynamical mass of $M_{\rm dyn} = 2.6 \times 10^{10}$ M$_\odot$. Using this estimation we calculate a gas mass fraction of $f_{\rm gas} = M_{\rm H_2}/M_{\rm dyn} \approx 60\%$. This constrain the CO luminosity to molecular gas mass conversion factor to $\alpha \lesssim 1.4$ M$_\odot$ (K km s^{-1} pc^{-2})$^{-1}$, otherwise the molecuar gas mass would exceed the dynamical mass.

REFERENCES

31. Sanders, D., Scoville, N. & Soifer, B. Molecular gas in luminous infrared galaxies. *Astrophys. J.* **370** 158-171 (1991).
32. Solomon, P. *et al.* The Molecular Interstellar Medium in Ultraluminous Infrared Galaxies. *Astrophys. J.* **478**, 144-161 (1997).
33. Aravena, M. *et al.* A survey of the cold molecular gas in gravitationally lensed star-forming galaxies at z > 2. *Mon. Not. R. Astron. Soc.* **457**, 4406-4420 (2016).
34. Hughes, D. *et al.* The Large Millimeter Telescope. *SPIE.* **7733**, 12- (2010).
35. Wilson, G. *et al.* The AzTEC mm-wavelength camera. *Mon. Not. R. Astron. Soc.* **386** 807-818 (2008).
36. Erickson, N. *et al.* An Ultra-Wideband Receiver and Spectrometer for 74–110 GHz *ASPCS* **375** 71- (2007).
37. Scott, K. B. *et al.* AzTEC millimetre survey of the COSMOS field - I. Data reduction and source catalogue. *Mon. Not. R. Astron. Soc.* **385** 12225-2238 (2008).
38. Yun, M. *et. al.* Early Science with the Large Millimeter Telescope: CO and [C II] Emission in the z = 4.3 AzTEC J095942.9+022938 (COSMOS AzTEC-1). *Mon. Not. R. Astron. Soc.* **454**, 3485-3499 (2015).
39. Savitzky, A & Golay, M. Smoothing and differentiation of data by simplified least squares procedures. *Analytical Chemistry* **36** 1627-1639 (1964).
40. Smail, I. *et. al.* The potential influence of far-infrared emission lines on the selection of high-redshift galaxies. *Mon. Not. R. Astron. Soc. Lett.* **414**, L95-L99 (2011).
41. Spilker, J. *et. al.* ALMA Imaging and Gravitational Lens Models of South Pole Telescope-Selected Dusty, Star-Forming Galaxies at High Redshifts. *Astrophys. J.* **826**, 112- (2016).
42. Fudamoto, Y. *et al.* The most distant, luminous, dusty star-forming galaxies: redshifts from NOEMA and ALMA spectral scans. *Mon. Not. R. Astron. Soc.* accepted (2017).
43. Lutz, D. *et al.* The far-infrared emitting region in local galaxies and QSOs: Size and scaling relations. *Astron. Astrophys.* **591** 136- (2016).
44. Hodge, J. *et al.* Kiloparsec-scale Dust Disks in High-redshift Luminous Submillimeter Galaxies. *Astrophys. J.* **833** 103- (2016).
45. Gullberg, B. *et al.* The nature of the [C II] emission in dusty star-forming galaxies from the SPT survey. *Mon. Not. R. Astron. Soc.* **449** 2883-2900 (2015).
46. Silva, L. *et al.* Modeling the Effects of Dust on Galactic Spectral Energy Distributions from the Ultraviolet to the Millimeter Band. *Astrophys. J.* **509** 103-117 (1998).
47. Ivison, R. *et al. Herschel* and SCUBA-2 imaging and spectroscopy of a bright, lensed submillimetre galaxy at z = 2.3. *Astron. Astrophys. Lett.* **518** L35- (2010).
48. Michałowski, M., Hjorth, J. & Watson, D. Cosmic evolution of submillimeter galaxies and their contribution to stellar mass assembly. *Astron. Astrophys.* **514**, A67- (2010).
49. Pope, A. *et al.* Mid-Infrared Spectral Diagnosis of Submillimeter Galaxies. *Astrophys. J.* **675**, 1171-1193 (2008).
50. Kirkpatrick, A. *et al.* GOODS-*Herschel*: Impact of Active Galactic Nuclei and Star Formation Activity on Infrared Spectral Energy Distributions at High Redshift. *Astrophys. J.* **759**, 139- (2012).
51. Kennicutt, R. The Global Schmidt Law in Star-forming Galaxies. *Astrophys. J.* **498**, 541-552 (1998).
52. Kennicutt, R. and Evans, N. Star Formation in the Milky Way and Nearby Galaxies. *Ann. Rev. Astron. Astrophys.* **50**, 531-608 (2012).
53. Chabrier, G. The Galactic Disk Mass Function: Reconciliation of the Hubble Space Telescope and Nearby Determinations. *Astrophys. J.* **586**, L133-L136 (2003).
54. Salpeter, E. The luminosity function and stellar evolution. *Astrophys. J.* **121**, 161- (1955).

55. Dunne, L. & Eales, S. The SCUBA Local Universe Galaxy Survey - II. 450-μm data: evidence for cold dust in bright IRAS galaxies. *Mon. Not. R. Astron. Soc. Lett.* **327**, 697-714 (2001).
56. Chapin, E. *et al.* An AzTEC 1.1mm survey of the GOODS-N field - II. Multiwavelength identifications and redshift distribution. *Mon. Not. R. Astron. Soc. Lett.* **398**, 1793-1808 (2009).
57. Magnelli, B. *et al.* A *Herschel* view of the far-infrared properties of submillimetre galaxies. *Astron. Astrophys.* **539**, 155- (2012).
58. Simpson, J. *et al.* The SCUBA-2 Cosmology Legacy Survey: Multi-wavelength Properties of ALMA-identified Submillimeter Galaxies in UKIDSS UDS. *Astrophys. J.* **839**, 58- (2017).
59. da Cunha, E. *et al.* On the Effect of the Cosmic Microwave Background in High-redshift (Sub-)millimeter Observations. *Astrophys. J.* **766**, 13- (2013).
60. James, A., Dunne, L., Eales, S. & Edmunds, M. SCUBA observations of galaxies with metallicity measurements: a new method for determining the relation between submillimetre luminosity and dust mass. *Mon. Not. R. Astron. Soc. Lett.* **335**, 753-761 (2002).
61. Dunne, L. *et al.* Type II supernovae as a significant source of interstellar dust. *Nature.* **424**, 285-287 (2003).
62. da Cunha, E. *et al.* An ALMA Survey of Submillimeter Galaxies in the Extended Chandra Deep Field South: Physical Properties Derived from Ultraviolet-to-radio Modeling. *Astrophys. J.* **806**, 110- (2015).
63. Solomon, P. & Vanden Bout, P. Molecular Gas at High Redshift. *Ann. Rev. Astron. Astrophys.* **43**, 677-725 (2005).
64. Scoville, N. *et al.* ISM Masses and the Star formation Law at $z = 1$ to 6: ALMA Observations of Dust Continuum in 145 Galaxies in the COSMOS Survey Field. *Astrophys. J.* **820**, 83- (2016).
65. Papadopoulos, P. *et al.* The Molecular Gas in Luminous Infrared Galaxies. II. Extreme Physical Conditions and Their Effects on the X $_{co}$ Factor. *Astrophys. J.***751**, 10- (2012).
66. Engel, H. *et al.* Most Submillimeter Galaxies are Major Mergers. *Astrophys. J.***724**, 233-243 (2010).